Equivalent Magnetic Noise Analysis for a Tunneling Magnetoresistive Magnetometer

Junqi Gao, Jiazeng Wang, Ying Shen, *Member, IEEE*, Zekun Jiang, Yu Huang, and Qiang Yu

***Abstract*—Tunneling magnetoresistive (TMR) magnetic sensors are broadly applied in various fields. However, to further improve the limit of detection (LOD), it is highly desirable to realize and calculate the noise limits of such sensor systems. Thus, techniques for noise elimination can be developed. In this paper, we propose an equivalent magnetic noise model to describe the LOD of a TMR magnetometer by considering intrinsic noise sources in the TMR sensing element and readout electronics. According to the model, the contribution of each noise source can be directly obtained. Therefore, the LOD of the magnetometer can be established theoretically. Moreover, the predicted detectivity of 390 pT/√Hz is also demonstrated by the experimental results. The model is applicable to all kinds of TMR sensors with a "Wheatstone bridge" configuration.**

***Index Terms*—TMR, readout electronics, noise model, LOD.**

I. Introduction

HIGH performance magnetometers are widely used in the area of weak magnetic field detection, such as magnetic anomaly detection (MAD) and biomedical imaging [1], [2]. Generally, the sensitivities of such magnetometers are in the range of fT to a few pT [3], such as those of superconducting quantum interference devices (SQUIDs), optically pumped magnetometers, search coils and fluxgates [4]. However, there are some drawbacks to these high-end magnetometers. For example, SQUIDs require extremely low operational temperatures [5], fluxgates have magnetic hysteresis and offset values under zero field [6], and optically pumped magnetometers consume considerable power [7].

Manuscript received June 8, 2020; revised June 28, 2020; accepted July 4, 2020. Date of publication July 8, 2020; date of current version August 26, 2020. This work was supported in part by the Stable Supporting Fund of Acoustic Science and Technology Laboratory under Grant JCKYS2019604SSJS005 and Grant JCKYS2020604SSJS006, in part by the Natural Science Foundation of Heilongjiang Province of China under Grant LH2019E040, and in part by the Academy of Space Electronic Information Technology under Grant 6142411183410. The review of this letter was arranged by Editor B. G. Malm. *(Corresponding authors: Ying Shen; Qiang Yu.)*

Junqi Gao, Jiazeng Wang, Ying Shen, and Zekun Jiang are with the Acoustic Science and Technology Laboratory, Harbin Engineering University, Harbin 150001, China, also with the Key Laboratory of Marine Information Acquisition and Security, Ministry of Industry and Information Technology, Harbin Engineering University, Harbin 150001, China, and also with the College of Underwater Acoustic Engineering, Harbin Engineering University, Harbin 150001, China (e-mail: shenying@hrbeu.edu.cn).

Yu Huang is with the Acoustic Science and Technology Laboratory, Science College, Harbin Engineering University, Harbin 150001, China.

Qiang Yu is with the Acoustic Science and Technology Laboratory, Harbin Engineering University, Harbin 150001, China, and also with the College of Automation, Harbin Engineering University, Harbin 150001, China (e-mail: yuqiang@hrbeu.edu.cn).

Color versions of one or more of the figures in this letter are available online at http://ieeexplore.ieee.org.

Digital Object Identifier 10.1109/LED.2020.3007950

Benefiting from the compact size, low cost and high power efficiency, MEMS magnetometers offer alternative solutions for various magnetic sensing applications [8]–[12], such as Hall sensors, magnetoresistance (MR) sensors and magnetoelectric (ME) sensors. Unfortunately, limited by the intrinsic noise, the LODs of available MEMS magnetometers are not suitable for weak magnetic field detection. Thus, recent investigations have focused on the design and optimization of MEMS sensors to enhance the magnetic field detectivity [13]–[15]. Among these solutions, a TMR magnetometer is perhaps one of the best candidates for ultralow magnetic field sensing [16], [17], which has been proved to have the capability of sensing magnetic fields down to the hundreds of pT level [2], [18]. To further enhance the detectivity, it is quite important to determine the noise sources of the TMR magnetometer. However, previous reports have mainly focused on the noise mechanism of magnetic tunneling junctions (MTJs) [19], [20]. Since they do not consider the noise of readout electronics, such works cannot be used to predict the LOD of TMR magnetometers directly.

In this paper, we establish an equivalent magnetic noise model to estimate the LOD of a TMR magnetometer, which deduces the noise sources in the TMR sensing element and readout circuit. More importantly, the most significant noise source of the device can be obtained directly. The predicted LOD shows agreement with the experimental results. Accordingly, noise elimination technology can be implemented to optimize the performance of TMR magnetometers in the future.

II. TMR Magnetometer Design

A. TMR Sensing Element

An MTJ multilayer was prepared by a multisource magnetron sputtering system with a base vacuum of 2×10^{-8} torr. In detail, the bottom electrode was fabricated by depositing Ta and Ru multilayers on a Si/SiO_2 substrate. An antiferromagnetic layer of IrMn was then formed to pin a CoFe layer. Then, a CoFeB layer was antiferromagnetically coupled to CoFe via a thin Ru layer. After that, a MgO barrier layer, a CoFeB free layer and a top electrode were deposited sequentially. The MTJ stacking structure is shown in Fig. 1 (a): thicknesses (in unit of Å) of the critical layers are marked.

The TMR sensing element was then fabricated by integrating hundreds of such MTJs to obtain a "Wheatstone bridge" configuration. To generate a differential output, the magnetization directions were varied between the arrays of MTJs, as shown in Fig. 1 (b). An image of the fabricated TMR sensing element and functional pads are indicated in Fig. 1 (c): such functional pads are eventually connected to four pins of an electronic package through wire bonding technique.

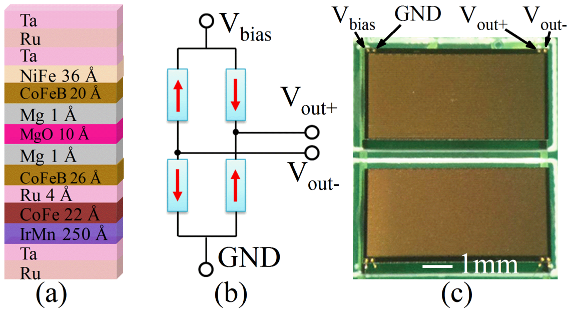

Fig. 1. (a) Schematic of the MTJ stacking; (b) electronic connection of the TMR sensing element; and (c) image of the TMR sensing element.

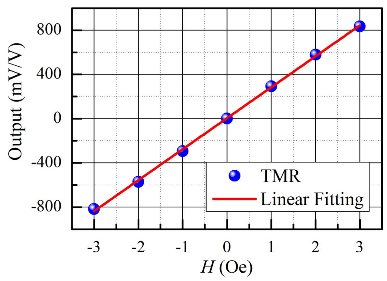

Fig. 2. Output signal of the TMR sensing element as a function of the magnetic field.

After processing, the sensitivity of the TMR sensing element was first characterized. During the measurement, the TMR sensing element was placed inside H-coils with a bias voltage of 1 V. The output signal of the TMR sensing element was then measured by changing the external DC magnetic field from −3 to 3 Oe. From Fig. 2, it can be seen that the sensing element exhibits great linearity in this field range, and the value of the sensitivity is determined to be 280 mV/V/Oe.

B. Readout Circuit Design

To capture the differential output generated by the TMR sensing element, classic instrumentation amplifier circuits were implemented to serve as readout electronics. Specifically, the circuit was designed to have a 4th-order low pass filter to eliminate the influence of noise above 10 Hz. Fig. 3 presents the simulated and measured transfer functions of the readout circuit, which show a uniform gain factor in a frequency range of 0.8 Hz to 10 Hz. The following section discusses the noise sources of this unit.

III. Results and Discussions

A. Noise Model for the TMR Sensing Element

To fully understand and estimate the TMR magnetometer noise level, a model for the TMR sensing element needs to be established first. To characterize the noise spectral density, the TMR sensing element was placed inside a magnetically shielded chamber to eliminate the interference from external magnetic fields. Then, the intrinsic voltage noise spectral density (SD) was captured by a dynamic signal analyzer (SR785, US). During the test, the TMR sensing element was powered by 5 volts, and the noise spectral density was measured with 50 times averaging. Moreover, the frequency spans were set as 100 Hz and 12.8 kHz separately, to obtain finer resolution over the frequency range of 0.8 Hz to 10 kHz.

From Fig. 4, it can be seen that the TMR sensing element shows $1/f$-type noise in this frequency range. The results

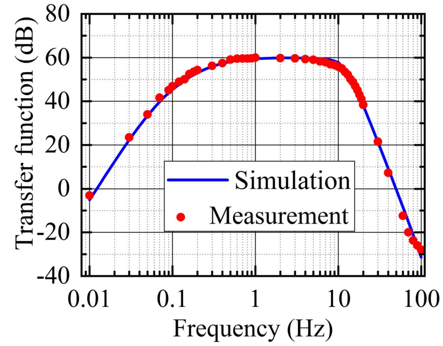

Fig. 3. Simulated and measured transfer functions of the circuit.

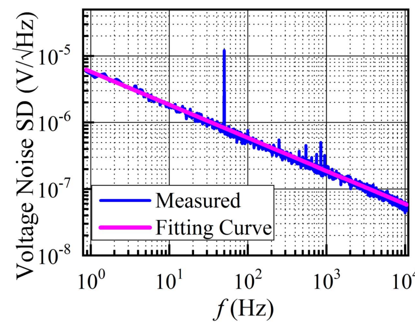

Fig. 4. Voltage noise SD of the TMR sensing element.

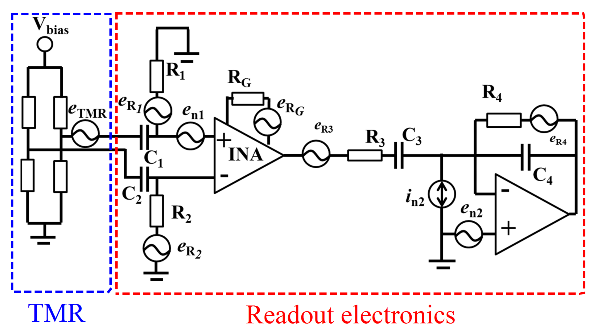

Fig. 5. Equivalent circuit noise model of the TMR magnetometer.

indicate that the noise is dominated by magnetic $1/f$ noise originating from magnetic domain fluctuations and electric $1/f$ noise originating from resistance fluctuations [21].

To describe the noise, a fitting curve modeled by employing the equation $N = A/f^B$ was used [22], where N is the fitting noise spectrum, A is the noise density index at a frequency of 1 Hz, f is the frequency and B is the frequency index referring to the noise attenuation rate with increasing frequency.

By fitting the measured curve, the A index is determined to be 5.8×10^{-6}. This suggests that the noise SD of the TMR sensing element at 1 Hz is 5.8 $\mu V/\sqrt{}$Hz, and the frequency index B is found to be 0.497.

B. Equivalent Circuit Noise Model

After investigating the noise characteristics of the TMR sensing element, the complete equivalent circuit noise model was established. It includes the TMR sensing element and readout electronics, as shown in Fig. 5. For the TMR part, the noise is described by a voltage source e_{tmr}, and the thermal noise from the resistors, the current and the voltage noise from the op-amps are considered in the readout electronics.

To calculate the PSD for each noise source, the transfer functions of the circuit in units of V/V need to be determined

TABLE I
VOLTAGE NOISE SD OF VARIOUS SOURCES

Source	Voltage Noise SD (V/√Hz)	Expression
TMR	*1/f noise* $\sqrt{e_{tmr}^2(f)}$	$\frac{5.8\times10^{-6}}{f^{0.497}}$
High pass filter	R_i-thermal noise (i=1,2) $\sqrt{N_{R_i}^2(f)}$	$\frac{\sqrt{4k_bTR_i}}{\lvert H_1(s)\rvert}$
INA	R_G-thermal noise $\sqrt{N_{R_G}^2(f)}$	$\frac{\sqrt{4k_bTR_G}}{\lvert H_1(s)\rvert}$
	e_{n1}-voltage noise of AD8422 $\sqrt{N_{e_{n1}}^2(f)}$	$\frac{e_{n1}}{\lvert H_1(s)\rvert}$
Bandpass filter	R_3-thermal noise $\sqrt{N_{R_3}^2(f)}$	$\frac{\sqrt{4k_bTR_3}}{\lvert H_1(s)\rvert\times G}$
	R_4-thermal noise $\sqrt{N_{R4}^2(f)}$	$\frac{\sqrt{4k_bTR_4}}{\lvert H_1(s)\rvert\times\lvert H_2(s)\rvert\times G}$
	i_{n2}-current noise of LMC6442	$\frac{i_{n2}\times Z_4}{\lvert H_1(s)\rvert\times\lvert H_2(s)\rvert\times G}$
	e_{n2}- voltage noise of LMC6442	$\frac{e_{n2}(\frac{Z_3+Z_4}{Z_3})}{\lvert H_1(s)\rvert\times\lvert H_2(s)\rvert\times G}$

TABLE II
NOISE CHARACTERISTICS OF AD8422 AND LMC 6442

Op-amp	$e_{n,1Hz}$ (nV/√Hz)	$e_{n,1000\ Hz}$ (nV/√Hz)	i_n (fA/√Hz)
AD8422 [a)]	10	8	80
LMC6442 [b)]	220	83	0.2

a) Cited from AD8422 Operational Amplifier, Analog Devices
b) Cited from LMC 6442 Operational Amplifier, Texas Instruments

first, including those of the RC high pass filter, instrumentation amplifier and bandpass filter. For the RC high pass filter, the function can be expressed as:

$$H_1(s) = \frac{sR_1(R_2)C_1(C_2)}{1 + sR_1(R_2)C_1(C_2)} \tag{1}$$

where $R_1(R_2)$ and $C_1(C_2)$ are the resistor and capacitor used in the high pass filter part, respectively, and s is a complex frequency.

Following the high pass filter, an AD8422 IC is used to serve as an INA that can amplify the differential signal induced by the TMR sensor. The gain factor (G) can be directly obtained from its datasheet:

$$G = \frac{19.8k\Omega}{R_G} + 1 \tag{2}$$

where R_G is the resistor used for gain selection.

Finally, a bandpass filter is implemented. The transfer function can be written as:

$$H_2(s) = -\frac{R_4}{R_3}\frac{R_4C_4s}{R_3C_3s+1}\frac{1}{R_4C_4s+1} \tag{3}$$

After obtaining the transfer functions, the referred-to-input (RTI) noise for all sources is summarized in Table I.

Where k_b is the Boltzmann constant, T is the absolute temperature, and $e_n = (e_{n,1Hz} - e_{n,1kHz})/f + e_{n,1kHz}$.

The detailed electronic properties of the op-amps are listed in Table II.

According to the theoretical expressions, the voltage noise SD of all sources can be calculated, as shown in Fig. 6 (a).

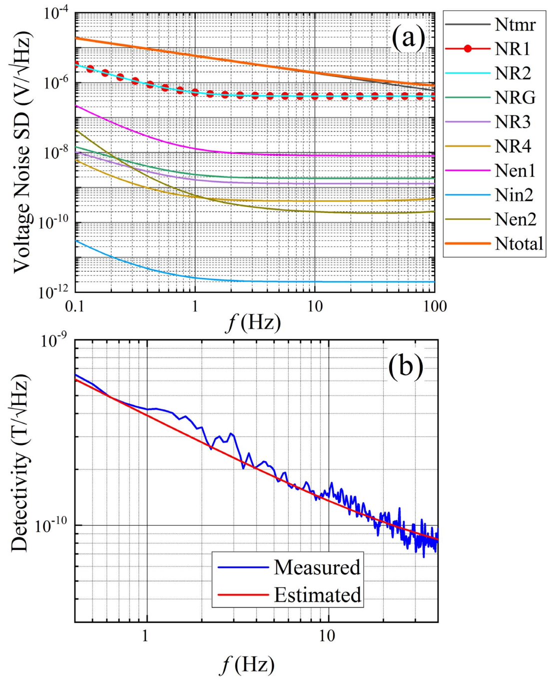

Fig. 6. (a) Simulation of voltage noise SD for various noise sources; (b) estimated and measured magnetic field detectivity of the TMR magnetometer.

Clearly, the most significant contribution to the total noise of this magnetometer is from the TMR sensing element in the frequency range of < 100 Hz; however, the thermal noise from R_1 and R_2 would become dominant sources above 100 Hz.

To evaluate the estimated results, the intrinsic noise of the TMR magnetometer was characterized by using the same setup as mentioned above. The voltage noise SD of the TMR magnetometer was directly captured by the DSA in the frequency range of < 100 Hz, in units of V/$\sqrt{}$Hz. To obtain the detectivity in units of T/$\sqrt{}$Hz, the following equation was used:

$$Detectivity(T/\sqrt{Hz}) = \frac{VoltageNoiseSD(V/\sqrt{Hz}) \times 10^{-4}}{Sensitivity(mV/V/Oe) \times V_{bias}(V)} \tag{4}$$

The detectivity of the TMR magnetometer after conversion is shown in Fig. 6 (b). One can see that the proposed model can estimate the noise behavior of the TMR magnetometer precisely over the frequency range of 0.8 to 10 Hz. The detectivity of this magnetometer is determined to be 400 pT$\sqrt{}$Hz at 1 Hz theoretically and experimentally.

IV. CONCLUSION

In summary, a noise model is proposed to analyze the noise sources of a TMR magnetometer, which has been demonstrated to have the capability of predicting the LOD of the TMR magnetometer accurately based on the experimental results. More importantly, the model can simulate the most significant noise sources, including the TMR sensing element and readout electronics. From the simulation, it is noted that the readout electronics may also limit the detectivity of the device. Therefore, more works should be performed to eliminate the low frequency noise of TMR magnetometers in the future.

REFERENCES

[1] A. Sheinker, L. Frumkis, B. Ginzburg, N. Salomonski, and B.-Z. Kaplan, "Magnetic anomaly detection using a three-axis magnetometer," *IEEE Trans. Magn.*, vol. 45, no. 1, pp. 160–167, Jan. 2009, doi: 10.1109/Tmag.2008.2006635.

[2] R. C. Chaves, P. P. Freitas, B. Ocker, and W. Maass, "Low frequency picotesla field detection using hybrid MgO based tunnel sensors," *Appl. Phys. Lett.*, vol. 91, no. 10, Sep. 2007, Art. no. 102504, doi: 10.1063/1.2775802.

[3] E. Mehdizadeh, V. Kumar, and S. Pourkamali, "Sensitivity enhancement of lorentz force MEMS resonant magnetometers via internal thermal-piezoresistive amplification," *IEEE Electron Device Lett.*, vol. 35, no. 2, pp. 268–270, Feb. 2014, doi: 10.1109/LED.2013.2293349.

[4] J. Lenz and S. Edelstein, "Magnetic sensors and their applications," *IEEE Sensors J.*, vol. 6, no. 3, pp. 631–649, Jun. 2006, doi: 10.1109/jsen.2006.874493.

[5] H.-J. Barthelmess, M. Halverscheid, B. Schiefenhovel, E. Heim, M. Schilling, and R. Zimmermann, "Low-noise biomagnetic measurements with a multichannel DC-SQUID system at 77 k," *IEEE Trans. Appiled Supercond.*, vol. 11, no. 1, pp. 657–660, Mar. 2001, doi: 10.1109/77.919430.

[6] Y. Shen, D. Ma, and J. Gao, "A man-portable magnetoelectric DC magnetic sensor with extremely high sensitivity," *IEEE Electron Device Lett.*, vol. 39, no. 9, pp. 1417–1420, Sep. 2018, doi: 10.1109/Led.2018.2858280.

[7] D. Viehland, M. Wuttig, J. McCord, and E. Quandt, "Magnetoelectric magnetic field sensors," *MRS Bull.*, vol. 43, no. 11, pp. 834–840, Nov. 2018, doi: 10.1557/mrs.2018.261.

[8] J. Vyhnánek, M. Janošek, and P. Ripka, "AMR gradiometer for mine detection," *Sens. Actuators A, Phys.*, vol. 186, pp. 100–104, Oct. 2012, doi: 10.1016/j.sna.2012.03.007.

[9] G. Y. Tian, A. Al-Qubaa, and J. Wilson, "Design of an electromagnetic imaging system for weapon detection based on GMR sensor arrays," *Sens. Actuators A, Phys.*, vol. 174, pp. 75–84, Feb. 2012, doi: 10.1016/j.sna.2011.11.034.

[10] Z. Chu, W. Shi, H. Shi, Q. Chen, L. Wang, M. J. PourhosseiniAsl, C. Xiao, T. Xie, and S. Dong, "A 1D magnetoelectric sensor array for magnetic sketching," *Adv. Mater. Technol.*, vol. 4, no. 3, Mar. 2019, Art. no. 1800484, doi: 10.1002/admt.201800484.

[11] J. Gao, J. Wang, L. Zhang, Q. Yu, Y. Huang, and Y. Shen, "Magnetic signature analysis for smart security system based on TMR magnetic sensor array," *IEEE Sensors J.*, vol. 19, no. 8, pp. 3149–3155, Apr. 2019, doi: 10.1109/JSEN.2019.2891082.

[12] W. Su, Z. Wang, T. Wen, Z. Hu, J. Wu, Z. Zhou, and M. Liu, "Linear anisotropic magnetoresistive sensor without barber-pole electrodes," *IEEE Electron Device Lett.*, vol. 40, no. 6, pp. 969–972, Jun. 2019, doi: 10.1109/LED.2019.2913506.

[13] S. Ikeda, J. Hayakawa, Y. Ashizawa, Y. M. Lee, K. Miura, H. Hasegawa, M. Tsunoda, F. Matsukura, and H. Ohno, "Tunnel magnetoresistance of 604% at 300K by suppression of ta diffusion in CoFeB/MgO/CoFeB pseudo-spin-valves annealed at high temperature," *Appl. Phys. Lett.*, vol. 93, no. 8, Aug. 2008, Art. no. 082508, doi: 10.1063/1.2976435.

[14] N.-N. Yang, X. Chen, and Y.-J. Wang, "Magnetoelectric heterostructure and device application," *Acta Phys. Sinica*, vol. 67, no. 15, 2018, Art. no. 157508, doi: 10.7498/Aps.67.20180856.

[15] Y. Wu, L. Xiao, S. Hou, Z. Gao, and L. Han, "High tc TMR-superconducting mixed sensor: Fabrication and performance," *IEEE Trans. Appl. Supercond.*, vol. 29, no. 1, pp. 1–5, Jan. 2019, doi: 10.1109/TASC.2018.2867790.

[16] P. P. Freitas, R. Ferreira, S. Cardoso, and F. Cardoso, "Magnetoresistive sensors," *J. Phys., Condens. Matter*, vol. 19, p. 21, Apr. 2007, doi: 10.1088/0953-8984/19/16/165221.

[17] M. Wang, Y. Wang, L. Peng, and C. Ye, "Measurement of triaxial magnetocardiography using high sensitivity tunnel magnetoresistance sensor," *IEEE Sensors J.*, vol. 19, no. 21, pp. 9610–9615, Nov. 2019, doi: 10.1109/JSEN.2019.2927086.

[18] S. H. Liou, X. Yin, S. E. Russek, R. Heindl, F. C. S. Da Silva, J. Moreland, D. P. Pappas, L. Yuan, and J. Shen, "Picotesla magnetic sensors for low-frequency applications," *IEEE Trans. Magn.*, vol. 47, no. 10, pp. 3740–3743, Oct. 2011, doi: 10.1109/TMAG.2011.2157997.

[19] J. P. Valadeiro, J. Amaral, D. C. Leitao, R. Ferreira, S. F. Cardoso, and P. J. P. Freitas, "Strategies for pTesla field detection using magnetoresistive sensors with a soft pinned sensing layer," *IEEE Trans. Magn.*, vol. 51, no. 1, pp. 1–4, Jan. 2015, doi: 10.1109/TMAG.2014.2352115.

[20] J. Checinski, P. Wiśniowski, M. Frankowski, and T. Stobiecki, "Magnetic noise prediction and evaluation in tunneling magnetoresistance sensors," *Sensors*, vol. 18, no. 9, p. 3055, 2018, doi: 10.3390/s18093055.

[21] Z. Q. Lei, G. J. Li, W. F. Egelhoff, P. T. Lai, and P. W. T. Pong, "Review of noise sources in magnetic tunnel junction sensors," *IEEE Trans. Magn.*, vol. 47, no. 3, pp. 602–612, Mar. 2011, doi: 10.1109/TMAG.2010.2100814.

[22] F. N. Hooge, "1/f noise sources," *IEEE Trans. Electron Devices*, vol. 41, no. 11, pp. 1926–1935, Nov. 1994, doi: 10.1109/16.333808.